Atmos. Chem. Phys. Discuss., 7, 6737–6765, 2007
www.atmos-chem-phys-discuss.net/7/6737/2007/

Atmospheric Chemistry and Physics Discussions

Cirrus clouds in convective outflow during the HIBISCUS campaign

F. Fierli[1], **G. Di Donfrancesco**[2], **F. Cairo**[1], **M. Zampieri**[1,3], **and E. Orlandi**[1]

[1]Istituto di Scienze dell'Atmosfera e del Clima, CNR, Italy
[2]Ente Nazionale Energia e Ambiente, Dipartimento Clima, Italy
[3]Laboratoire de Meteorologie Dynamique, Ecole Normale Superieure, France

Received: 12 February 2007 – Accepted: 2 May 2007 – Published: 16 May 2007

Correspondence to: F. Fierli (f.fierli@isac.cnr.it)

Abstract

Light-weight microlidar measurements were taken on-board a stratospheric balloon during the HIBISCUS 2004 campaign, held in Bauru, Brazil (22 S, 49 W). Tropical cirrus observations showed high mesoscale variability in optical and microphysical properties. The cirrus clouds were observed throughout the flight between 12 and 15 km height. It was found that the clouds were composed of different layers, characterized by a marked variability in height, thickness and optical properties. Trajectory analysis and mesoscale transport simulations clearly revealed that the clouds had formed in the outflow of a large and persistent convective region, while the observed optical properties and cloud structure variability could be linked to different residence times of convective-processed air in the upper troposphere. Mesoscale simulations were able to reproduce the supersaturation due to recent outflow, while it was necessary to consider the presence of other formation processes than convective hydration for cirrus forming in aged detrained anvils.

1 Introduction

Upper tropospheric ice clouds in the tropics (tropical cirrus) have a major effect on the terrestrial climate. Cirrus cover up to 20% of the tropical region (Liou, 1986) and significantly impact on the Earth's radiative balance. They reduce the incoming solar radiation by reflection, and absorb upward the infrared radiation emitted in the lower atmosphere.

The result may be a reduction in the net outgoing longwave radiation, causing a heating of the atmosphere (Hartmann, 1993); such heating should be more efficient in the stratosphere if the impact of tropopause level tropical cirrus is included (Ackerman et al., 1988; Folkins and Martin, 2005). However, the effective impact of cirrus on the radiative balance depends also on several parameters, such as underlying surface conditions, cloud height and thickness, and ice crystal size distribution.

Deep convection transports moist air from the ground to the upper troposphere and cirrus can easily form in the moist cloud outflow. In turn, the cirrus remove humidity through crystal formation and sedimentation, thus influencing the water vapour budget in the tropical tropopause layer (TTL). Although it is well known that air enters the stratosphere after upwelling in the tropics, the mechanism of upward transport in the TTL is still uncertain. In fact, the main outflow of tropical deep convection is found at around 13 km height (350 K potential temperature). Gettelman et al. (2002) show that convective overshooting episodes are too rare and do not transport enough mass to supply the Brewer Dobson circulation. Nevertheless, recent analysis of tropical observations from HIBISCUS and TROCCINOX (TROpical Convection CIrrus and Nitrous OXydes experiment) campaigns indicates that convective overshooting might play an important role on the vertical transport at the tropical tropopause (Pommereau et al., 2007, Chaboureau et al., 2006)

Additional vertical transport in the TTL is provided by diabatic air mass lifting or descent induced by the radiative impact of cirrus. Nonetheless, a definitive picture of motion related to radiation-cloud interaction is as yet unclear. Fueglistaler and Fu (2006), using Atmospheric Radiation Measurement (ARM) cloud measurements in the tropics, estimate that increased short-wave radiation reflected by high clouds is compensated by reduced infrared radiation, resulting in a cooling effect in the lower stratosphere. The modelling experiments of Corti et al. (2006) indicate that cirrus cloud-radiation interaction can offer a pathway for upward mass transport in the tropical tropopause region.

All these processes are strongly dependent on cloud persistence, spatial and vertical extension, and particle size distribution. Therefore, it is important to characterize the microphysical properties of upper tropospheric ice clouds, and to shed light on mechanisms leading to their formation. The processes involved in the formation and maintenance of tropical cirrus are not completely understood, because few detailed measurements of their microphysical properties are available.

The APE-THESEO observations (Airborne Platform for Earth research-THird Euro-

pean Stratospheric Experiment on Ozone) show that upper tropospheric cirrus forms in in the outflow of deep convective clouds followed by slow synoptic uplifting or by mesoscale lifting of water vapour driven by turbolence induced by convective gravity waves Santacesaria et al. (1992). Optically thin layers of small crystals can persist at the tropopause level for a time ranging from several hours to few days (Luo et al., 2003). Subvisible cirrus absorbs infrared radiation and may induce uplifting of air, with ascending speeds in the order of mm/s^{-1}. Tropical subvisible cirrus clouds may represent a sink for water entering the stratosphere, since cooling events of only few degrees may lead to growing large particles that sediment and dehydrate air before entering the stratosphere Peter et al. (2003).

The Center Equatorial Pacific Experiment (CEPEX) analysis (McFarquhar and Heymsfield, 1996) showed that the cirrus ice crystal dimension is related to the convective age, and that particles with larger radar cross-section are found nearer to the convective core. Pfister et al. (2001) identified two classes of cirrus from a comprehensive analysis of data from the Tropical Ozone Transport Experiment/Vortex Ozone Transport Measurement (TOTE/VOTE) experiment. One class appears to be related to particle and water vapour detrainment due to convection. However, it is also evident that cirrus layers must be maintained by dynamical or radiative processes. The second class of clouds is related to deep convection hydration, but their formation is not directly linked to convective outflow. The presence of two cirrus cloud classes related to distinct formation processes was also identified in the APE-THESEO observations by Mackenzie et al. (2006). Massie et al. (2002) combined extinction data obtained by the Halogen Occultation Experiment (HALOE) and trajectories from the European Center for Medium range Weather Forecasting (ECMWF). They found that half of the HALOE cirrus observations in the maritime continent are related to deep convection detrainment, while the remaining part is likely to be formed by in-situ processes.

The task of the present paper is to identify convection as the formation mechanism of tropical cirrus clouds observed by ballonborne-lidar, and to correlate their differences in microphysics with the variability of airmass convective processing. Trajectory analysis

and mesoscale modelling are used to interpret the cirrus microlidar optical observations acquired on a stratospheric balloon in the framework of the 2004 HIBISCUS campaign (Pommereau et al., 2007). The balloons were launched from Bauru (22 S, 49 W) during the 2004 wet season. The HIBISCUS measurements were taken above the South-American continental region, where deep convection is often observed (Liu and Zipser, 2005). Cirrus measurements were performed on 24 February, from 22:00 UTC during the Short duration Flight Number 4 (SF4). Trajectories are used to correlate the observed clouds to the active convective regions, while mesoscale meteorological models are analysed to estimate the convective age of the clouds and correlate it with observed optical properties.

Section 2 presents the microlidar observations, an outline of the retrieved variables and a description of the synoptic situation based on satellite measurements. Section 3 describes the synoptic trajectory analysis, while Sect. 4 describes the mesoscale model simulations performed to estimate the convective age of the cirrus layers. The main findings of the paper are outlined in the Conclusions.

2 Observations

2.1 Satellite observations

Persistent convective activity was recorded in central Brazil during the three days prior to the SF4 balloon flight. The South-America continental region was characterized by a positive precipitation anomaly during February 2004. In particular, from 20 to 24 February, the region of Bauru was under the influence of the South America Convergence Zone (SACZ). The SACZ gives rise to a large region of intense convection originating from the Amazon basin and extending south-eastward.

The first row of Fig. 1 reports the GOES-12 (Geostationary Operational Environment Satellite) measurements of the infrared radiative temperature from the 10.7 μm channel every 12 h from 22 February at 14:45 UTC to 24 February at 14:45 UTC. The structure

of large scale convection and wet air outflow in the SACZ can easily be seen. Convection develops in the nighttime during the days prior to the SF4 flight in a vast region north-east of Bauru. Convective systems are triggered corresponding to an intense frontal interface, directed NW-SE, which approximately extends from the center of the analyzed domain to its SSE boundary. Convective activity has a clear diurnal cycle on 22 and 23 February, while GOES measurements from 14:45 UTC on 24 February show that convection develops earlier than on the previous two days.

Additional information on the cloud type and the outflow structure comes from the observations of the Moderate Infrared Spectrometer (MODIS) onboard the TERRA satellite. MODIS provides an estimate of Cloud Top Pressure (CTP) and optical thickness in nadir geometry (see King et al., 1997 for details). The closest overpasses were at 13:50 UTC on 24 February (11 h before the SF4) and at 02:50 UTC on 25 February (4 h after SF4). The observations are reported in Fig. 2, where only clouds with top pressure above 350 hPa pressure level are plotted. From a comparison among ground-based radar observations, MODIS data show a positive bias in optical thickness and underestimate cloud top height (Mace et al., 2005). Dessler and Yang (2003) discussed the cloud parameter uncertainty and estimated thin tropical cirrus distribution based on optical thickness from MODIS Terra 1.375 μm channel. Since MODIS observations were not simultaneous with SF4, it is not possible to correlate them directly with lidar observations to infer additional information on observed clouds. Nevertheless, the presence and the extension of optically thin clouds in the convective outflow can complement the information obtained from the GOES data analysis. On 24 February (Fig. 2 left panels) a large convective region is visible NE of the balloon measurement site, with several convective towers reaching a CTP lower than 150 hPa (red areas). The overall structure of the convective systems agrees well with the GOES observation at 14:45 (Fig. 1, top right panel). Aerosol optical thickness (Fig. 2, left panel) also shows that convective clouds are optically thick (up to 1), while the western flank of the convective region (55 W, 15 S to 44 W, 28 S) is characterized by a large and elongated cloud with optical thickness lower than 0.2 and top height between 250 and 150 hPa. This can

be interpreted as a clear signature of cirrus generated from the outflow of convective systems, transported south-eastward by the upper tropospheric jet at the west side of the SACZ. Data from the following day (Fig. 2, right column) show the presence of large convective systems at 18 S latitude and smaller cloud systems east of Bauru. The SF4 region (enclosed in the black box in Fig. 2) is characterized by optically thick clouds at variable height, but it is not possible to discriminate the presence of cirrus cloud since they could have been masked by thicker clouds at a lower altitude. The combination of GOES and MODIS images suggests that during the SF4 flight, the upper troposphere was clearly perturbed by ubiquitous and persistent convection where large cirrus clouds formed. It is likely, therefore, that the region sampled by the microlidar was influenced both by recent (up to 1 day) and aged (up to 3 days) convective outflow. Nevertheless, due to the MODIS time coverage, it cannot be demonstrated that cloud particles were present throughout the outflow from convective uplift to the observation time. Additional details of the synoptic situation from TRMM (Tropical Rainfall Measurements Mission) for the 20–24 February period are given in two papers (Marecal et al., 2006 and Huret et al., 2007[1])

2.2 Balloon-borne microlidar

The lightweight microlidar made observations during flight SF4; the balloon was launched at 20:00 UT (18:00 local time) on 24 January 2004 and terminated at 01:00 UT the following day (23:00 local time). The lidar measurements, shown in Fig. 3, were taken at the end of the balloon floating (22:00 UT) and during the first part of the descent, crossing the cirrus cloud between 00:00 UTC and 00:40 UTC on 25 February (visible as an abrupt measurement stop in Fig. 3). The instrument acquires a vertical profile each 20 s with a horizontal resolution of 2 km, given a constant drift

[1]Huret, N. Durry, G. Riviere, E. D., et al.: In-situ laser diode measurements of H2O during the HIBISCUS campaign. Part 3: Investigation of convective event impact on the TTL water vapor content, Atmos. Chem. Phys. Discuss., in preparation, 2007.

speed of the balloon, and the vertical resolution is 15 m. Details of the instrumental set-up are given in Di donfrancesco et al. (2006).

The microlidar measures backscatter at parallel and perpendicular polarization at 532 nm wavelength. The backscatter ratio is defined as the ratio between the total backscattered radiation and the molecular backscatter:

$$\mathrm{BSR} = \frac{\beta_m + \beta_a}{\beta_m} \tag{1}$$

β_m is the molecular backscatter and β_a is the aerosol backscatter. $\beta_m+\beta_a$ is proportional to the lidar signal while β_m is calculated from density profile measured by Bauru radiosounding. Aerosol backscattered light is split into parallel ($\beta_a^{\parallel}$) and perpendicular ($\beta_a^{\perp}$) polarization. Aerosol depolarization is defined as the ratio between the two components:

$$D = 100\frac{\beta_a^{\perp}}{\beta_a^{\parallel}} \tag{2}$$

Values of D above zero imply that emitted light scatters over aspherical particles. Typical values of D, in the presence of solid aerosols ranges from 10% to 70% and different values of D are related to different scatterer dimensions and shapes. Thus, D is used to identify the presence of particles in the ice phase and, coupled with BSR, to classify clouds in a qualitative way. The time vs. height evolution of BSR and D from flight SF4 are plotted in Fig. 3 (upper panel and lower panel). Three distinct layers can be identified: (1) thick cirrus characterized by high BSR (up to 30) and low aerosol depolarization values (D<20%) at around 13 km height during the first half of the flight (in the blue box in Fig. 3, top panel); (2) thick cirrus, with similar BSR and D values to layer (1) in the second part of the flight at 12 km height (violet box); (3) thinner cirrus with low BSR (<20) and high D values (D>30%) cirrus layers between 13 and 15 km height during the second part of the flight (orange box).

Micro-SDLA (balloon-borne diode laser spectrometer) measurements of water vapour mixing ratio from Durry et al. (2006) during the SF4 descent (25 February 01:00 UT) indicate that superaturation reaches 130% throughout the layer where cirrus were observed during SF4 floating.

The different layers can be identified in Fig. 3 (lower panel), which reports the D average with its standard deviation for each unit of BSR; the colors correspond to layers 1–3. It can be seen that the optical properties of layers 1 and 2 (blue and violet lines) are similar, with a large range of BSR values (1 to 60) and quasi-constant D for BSR larger than 20. Layer 3 (orange line) has BSR values ranging between 1 to 10, with higher values of D. In general, D increases with BSR increasing up to 10.

It should be noted that layer 2 has coherent undulation in BSR intensity between 23.1 S and 22.8 S (23:00 UTC and 23:55 UTC), with an apparent horizontal wavelength in the order of 60 km and vertical displacement of BSR maxima of 600 m. These values lies within the range of gravity waves observed in the vicinity of convective systems (Pfister et al., 2001) and tropopause folding (Cho et al., 1999). The analysis of meteorological parameters on-board the balloon (not reported) show the presence of a coherent wave structure during the first part of the descent (between 23:30 and 00:20 UTC on 25 January) with peak-to-peak temperature amplitude of 1 K, apparent horizontal wavelength of 25 km and vertical wavelength of 100 m. The vertical displacement associated to the wave is around 300 m. The lack of accurate in-situ wind observation do not allow to infer additional properties of the observed wave structure.

The differences in optical properties are certainly related to the different properties of the scatterers. On the basis of the satellite observations, it can also be hypothesized that cloud particle variability is linked to the microphysical processes in convective outflows. Several studies have tried to identify a functional relationship between lidar observed parameters (as D) and scatterer microphysical properties. The modelling approach of Liu and Mishchenko (2001) shows that lidar depolarization values are related to the shape of cloud particles, but are not representatives of the particles size in the micrometric range. Sassen and Benson (2001) demonstrate that depolarization

can be linked to the local temperature to infer transition in cirrus ice crystal shape and internal crystallographic features. Noel et al. (2004), combining simultaneous lidar and in-situ observations, propose a correlation between depolarization and particle shape typologies. Whiteway et al. (2004) identify the crystal families that form in different positions with respect to the convective core, using the in-situ observations from the EMERALD campaign (Egrett Microphysics Experiment with RAdiation, Lidar, and Dynamics). Nevertheless, in the authors point of view, the uncertainty remains too high to characterize quantitatively microphysical processes in convective outflow based solely on lidar observations. Therefore, the present work will focus rather on the correlation between observed cirrus mesoscale variability and macrophysical properties, such as cloud thermal history and airmass convective age (defined as the time elapsing between convective uplift and observation) as inferred from the ECMWF analysis and mesoscale modelling.

3 Trajectories

Since the position, temperature and humidity conditions experienced by air parcels are key parameters for cirrus formation, Lagrangian trajectories have been extensively used to assess water vapor transport and freezing in the TTL (see for example Fueglistaler et al., 2005), and to identify successfully different typologies of tropical cirrus (Pfister et al., 2001). Back-trajectory clusters are used here to identify the mechanisms leading to cirrus formation during flight SF4.

The trajectories are computed with the FLEXTRA model (Stohl et al., 1999) driven by the ECMWF T312 analysis at 0.5° horizontal resolution and 60 vertical hybrid levels. This leads to a horizontal resolution of 40 km and a vertical resolution from 500 m to 1000 m in the upper troposphere region. The vertical velocities used for three dimensional advection are estimated from the omega equation. Trajectories are calculated backward for 96 h at 22:00 UTC, 24 February, starting from a 2-D latitude-height array corresponding to the microlidar observation in Fig. 3; the resolution of the array is

10 km in the horizontal and 500 m in the vertical. Specific humidity is interpolated from the ECMWF analysis at each trajectory point.

The left panel of Fig. 4 shows the height and water vapor along the trajectories. On average, most air masses are subject to relatively rapid uplift, indicating that the cirrus layer could be generated by convective outflow. Three distinct periods of uplift can be identified 90, 60 and 40 h before measurement, well correlated with the nighttime maximum of convective activity shown in Fig. 1. As expected, the specific humidity decreases with height, and a small signal of hydration due to convective transport is visible for the last two uplift events. Additional information can be derived from the temperature and humidity conditions experienced by air masses. For this purpose, relative humidity with respect to ice (RH_i) is calculated for each trajectory using the formula prescribed by the World Meteorological Organization and the Marti and Mauersberger (1993) formula for ice saturation. The height and time where the condition of saturation with respect to ice is satisfied (RH_i>100%) are overlaid on the plot in Fig. 4. Saturation occurs during the uplift and persists for the subsequent 24 hours only for airmasses that experienced the most recent convective ascent. In fact, the condition of saturation only persists 60 h before the observation for the other air masses. It is also important to remark that during the 20 h prior to the measurement, RH_i never exceeds 100%.

The question arises of whether different uplift times can be correlated to observed optical differences in cirrus layers. In order to establish such a link, convective age (t_c) is estimated for each observation point; t_c is defined as the time when cirrus air masses irreversibly go above 9.5 km height. The plot of the t_c function of height and latitude is reported in the right panel of Fig. 4, which shows that t_c has a large variability with height. The layer above 13 km height experienced uplift between 30 to 40 h before measurement, the thicker intermediate layer between 55 to 65 h before measurement, and the lowermost layer 90 h before measurement. The combined analysis of RH_i and t_c shows that during SF4 the upper troposphere can be separated into layers characterized by well defined differences in convective age and thermal/saturation conditions: higher layers experienced more recent uplift and saturation, while convective age is

ACPD
7, 6737–6765, 2007

higher for lower layers.

The reader should be warned that FLEXTRA trajectory analysis may have important uncertainties. The ECMWF analysis has a water vapor dry bias in the upper troposphere (Tompkins et al., 2005), which is clearly reflected by the fact that the condition of saturation with respect to ice is not reached during the 20 h prior to SF4. The same authors have recently implemented a supersaturation scheme that reduced the humidity bias compared to in-situ measurements, which was not yet included in the ECMWF model version used for the analysis performed in this study. Additional uncertainty originates from the FLEXTRA vertical velocities, since the omega equation is calculated from the ECMWF divergence generated by explicit convection, which could lead to an underestimation of convective uplift.

4 Mesoscale simulation

4.1 Model description

Convective transport properties relative to flight SF4 are analysed with the BOLAM (BOlogna Limited Area Model) mesoscale model to extend and improve the qualitative view provided by the Lagrangian approach. BOLAM is a meteorological model based on primitive equations in the hydrostatic approximation. It uses wind components u and v, potential temperature θ, specific humidity q and surface pressure ps. The BOLAM version used here also includes the advection of passive tracers. Variables are defined on hybrid coordinates and are distributed on a non-uniformly spaced Lorenz grid. The horizontal discretization employs geographical coordinates, with latitudinal rotation on an Arakawa C-grid. The model implements a Weighted Average Flux (WAF) scheme for the three- dimensional advection. The lateral boundary conditions are imposed by means of a relaxation scheme that minimizes wave energy reflection (Davies, 1976; Lehman, 1993). Deep convection is parameterized with the scheme of Kain-Fritsch (Kain and Fritsch, 1990; Kain, 2004). The boundary layer scheme is based

on the mixing length assumption and on the explicit prediction of turbulent kinetic energy (Zampieri et al., 2005), while the surface turbulent fluxes are computed according to the Monin-Obukhov similarity theory. The parameterization of the effects of vegetation and soil processes (Pressman, 1994) is based on the water and energy balance in a four layer soil model, and includes the diagnostic computation of skin temperature and humidity, seasonally dependent vegetation effects, evapo-transpiration and interception of precipitation. The radiation is computed with a combined application of the scheme from Ritter and Geleyn (1992) and the operational one from the ECMWF (Morcrette et al., 1998). Further details of the model are given in Buzzi and Foschini (2000). In order to analyze the tracer distribution during flight SF4, the simulation starts 72 h before the observations (00:00 UTC on 22 February). The model has 60 vertical hybrid levels, from the ground to the top of the atmosphere (0.1 hPa), with denser levels near the ground, leading to a vertical resolution of 500 m in the upper troposphere. The horizontal domain has 240*140 grid points at 20 km of resolution.

4.2 Tracer Initialization

Several works have utilised mesoscale simulations of tracers to estimate transport in a single convective event (see for example Mullendore et al., 2005). Since the main goal of the present work is to correlate the observed cirrus optical properties with the air mass convective age, it is necessary to track the evolution of hydrated air lifted by convection at different times. In order to estimate the convective impact function of the simulation time, idealized tracer 3-D fields are analyzed together with specific humidity fields. To this end, three tracers are continuously emitted for 24 h at different times during the simulation: from the beginning to 24 (T0), from 24 h to 48 h (T24), and from 48 h to 72 h (T48). The tracers are kept at a constant concentration of 1 kg/kg at the ground level (2 m) after injection, thus representing a constant ground source. Each tracer is subject to turbulent transport, advection and convective re-adjustment. Tracers are non-soluble, and dry deposition processes are not considered since the objective is to diagnose the convective transport of boundary layer air in the upper troposphere.

Moreover, gravitational deposition is assumed to be negligible at the time-scale of a few days, on which this numerical study is focused; this hypothesis has been also discussed and validated in Mullendore et al. (2005).

4.3 Comparison with GOES data

The analysis of convective outflow transport requires accurate simulations of the life cycle, position and height of convective clouds. To evaluate BOLAM's accuracy by direct comparison with GOES-12 data, the cloud radiance temperature at 10.8 μm is estimated from model thermodynamical and cloud parameters with the RTTOV8.5 forward model (Saunders and Brunel, 2004).

The simulated cloud radiance temperature fields simultaneous to the satellite observations are reported in the bottom row of Fig. 1. The model convective activity is in good agreement with the GOES-12 observations. BOLAM reproduces well the large scale dynamics and the localization of the convergence region where most convection occurs. It is also worth noting that the comparison can be extended to the scale of the single convective system, since BOLAM reproduces the high clouds observed on the western side of the convergence zone on 23 February, 03:00 UTC, 24 February, 03:00 UTC and 15:00 UTC. At first glance, BOLAM simulations overestimate the radiance temperature (underestimate the cloud top height) with respect to the GOES data. Fig. 5 reports the high cloud fraction seen by GOES and BOLAM in the geographical domain of Fig. 1, where the radiance temperature maximum threshold of 240 K is used to select high clouds. Although BOLAM reproduces remarkably well the cloud cycle seen by GOES, with nighttime cloudiness maximum, it underestimates the area covered by high clouds during the first part of the simulation, while values quantitatively comparable with the GOES data are obtained for the last 30 h of the simulation.

The agreement between BOLAM and GOES observations on the position and lifetime of the main convective systems ensure the accurate reproduction of upper tropospheric tracer sources and large scale flow, while BOLAM positive bias in cloud top temperature could lead to an underestimation of the aged outflow height.

4.4 Tracer transport

The T0 concentration at 12 km at 22:00 UT on 24 February, reported in the left panel of Fig. 6, shows that the tracer emitted on 22 February impacts on a large area in the upper troposphere, even if it is highly diluted with respect to the ground concentration. A filament of higher concentration of T0 is located at the western flank of the convective region, intersecting with the SF4 flight path. The flight direction is shown by the yellow arrow in Fig. 3, while the measurement ranged between 23.5 S and 22.4 S. The T48 high concentration at 14 km (Fig. 6, left panel) is attributed to convection forming between 16 S and 20 S on 24 February (observed and simulated at 03:00 UTC in Fig. 1) and to convection developing south of 20 S during the afternoon of 24 February. The T48 concentration is higher than T0, due to the reduced dilution effect. Maximum concentrations reach values of 0.4 kg/kg, comparable to 1 kg/kg (emission level), indicating that, in the absence of removal processes, convective transport is highly efficient, and that SF4 is strongly influenced by more recent convection at 14 km height.

The left panel of Fig. 7 shows the relative humidity (RH) and ice supersaturation, while the right panel presents the T0 and T48 tracers along the section shown by the yellow arrow of Fig. 5. The cirrus observations lie between the yellow vertical bars. The relative humidity field is mainly controlled by recent convection developing in the northern part of the domain, with the nearest convective system (where RH exceeds 100 %) reaching 15 km height. The region where RH_i exceeds 130% is overlaid as crosses on the RH field in Fig. 7, where supersaturation threshold has been chosen for direct comparison with the SF4 SDLA humidity data shown in Marecal et al. (2006). The BOLAM simulations indicate the presence of supersaturation in the outflow between 12 and 14.5 km height, but do not show the presence of convective hydration below 12 km, where SDLA and lidar measure cirrus cloud in supersaturated air. The T0 tracer (right panel in Fig. 7) is well correlated with the RH field, with a high concentration in the convective cloud and in its outflow. The 0.15 kg/kg contour for T0, T24 and T48 is overlaid on the right panel in Fig. 7. T48 is concentrated in a 1 km thick layer

ACPD
7, 6737–6765, 2007

EGU

below the outflow. Together with the 2-D field in Fig. 6, it is possible to have a 3-D view of aged outflow transport: T48 is advected at the west side of the intense convection region and penetrates below the T0 layer uplifted by convection. T24 is present only in a thin layer at 8 km height. It should be also noted that the dry layer between 8 and 10 km height, with negligible tracer concentrations and RH less than 10%, can be interpreted as a stratospheric filament following the analysis from Durry et al. (2006).

The BOLAM simulation confirms the picture of hydrated air from recent outflow lying above a layer with higher convective age gained from trajectory analysis, and allows the identification of the large scale structure of convective processed air transport. Convective outflow uplifted 3 days before the SF4 flight is advected at the western flank of the convective region. At the same location the 24 February MODIS image reveals the presence of clouds with low optical thickness. BOLAM correctly estimates RH_i for the more recent outflow compared to observed values of RH_i in Durry et al. (2006). The same event was simulated with the mesoscale BRAMS model in Marecal et al. (2006), showing that the use of a simplified microphysical scheme leads to results comparable with BOLAM, while the simulations without microphysics could not reproduce supersaturation for the whole SF4 profile.

Therefore, it is possible to identify different mechanisms for the cirrus cloud generation. The higher cirrus layer (1) forms in the outflow adjacent to the convective system. Lower layer cirrus (2) could be explained as combination of airmass hydration by more aged convection and a local formation mechanism. The different optical properties of layer (3) with respect to (1) can be attributed to cirrus fading in sheared outflow. Therefore, optical properties rapidly evolve within 6 h during outflow transport, while cirrus in aged outflow could show similar optical properties to the cloud generated in the recent outflow. As a final inclusive point, it should be mentioned that the aged convection outflow height could be underestimated by the BOLAM model. In fact, the comparison with GOES data revealed that during the first part of the simulation BOLAM overestimates the cloud top temperature. This could imply that layers 1 and 2 both originate from recent convection, while layer 3 originates from older convection and should be

sustained by additional cooling. This suggests that optical properties are stable for the whole recent outflow, while they are subject to transition in the older outflow cirrus cloud.

5 Conclusions

Lidar observations from flight SF4 during the HIBISCUS campaign provide evidence of two distinct cloud types, based on their optical properties. The first class is characterized by higher values of BSR and lower values of D, while, for the second class, BSR has lower values and D higher values. The two types of clouds are observed at adjacent locations and at similar altitudes. From the D and BSR classification, both seem to fit the HACII typology proposed by Pfister et al. (2001).

The lidar data analysis suggests that the two types of cirrus clouds could be identified in terms of particle size and shape, reflecting different formation mechanisms and thermal histories. Satellite data analysis and transport modelling confirm the convective origin of the cirrus clouds. In fact, the flight SF4 was influenced by deep convection developing in a vast region north of Bauru, which uplifted moist air at different times.

While trajectory analysis fails to reproduce the observed humidity distribution, the mesoscale model simulation agrees well with the observed convection and with the observations of cirrus in supersaturated air above 12 km height. Nevertheless, despite the fact that the BOLAM estimate of convective age seems to be coherent with the whole cloud layering, the presence of cirrus clouds below 12 km height cannot be explained quantitatively by the simulated humidity field. Both pictures of cirrus formation provided by mesoscale modelling are consistent with the conclusions of Mace et al. (2006), who suggest that tropical cirrus originating from detrained anvils must be maintained by local processes that allow cloud particles to resist gravitational sedimentation. Pfister et al. (2001) suggest that an alternative mechanism enhancing outflow cirrus lifetime might be particle reformation in aged outflow, due to waves allowing supersaturation through local cooling.

ACPD
7, 6737–6765, 2007

The analysis presented here, although not as extensive as the one reported in Pfister et al. (2001), also suggests the presence of gravity waves a possible cause of temperature perturbation: the upper tropospheric shear shown by the tracer analysis could be an efficient wave source that induces the coherent structure also visible in the lidar BSR in Fig. 3. This analysis, following previous observational studies, confirms that cirrus clouds can have a complex structure on account of concurrent and partially unknown formation processes, which cannot be fully reproduced by state-of-the-art meteorological models. It should be stressed that the presence of an unpredicted cloud layer can have a strong impact on model estimates of the radiative and water vapor budgets in the upper troposphere. This implies that reliable estimates of cirrus optical thickness, geographical extension and height are crucial in the study of the upper troposphere and lower stratosphere climate systems and their feedbacks.

Acknowledgements. This study was supported by the EU through the HIBISCUS project of the VIFP. M. Viterbini and C. Buontempo are acknowledged for their support in the field campaign. The ECMWF is acknowledged for providing the atmospheric analysis used in this work. Finally, the authors wish to thank D. Brunner for providing the GOES data

References

Ackerman, T. P., Liou, K.-N., Valero P. J., and Pfister L.: Heating rates in tropical anvils, J. Atmos. Sci., 45, 1606–1623, 1988. 6738

Buzzi A. and Foschini L.: Mesoscale meteorological features associated with heavy precipitation in the southern Alpine region, Meteorol. Atmos. Phys., 72, 131–146, 2000. 6749

Chaboureau J.-P., Cammas J.-P., Duron J., Mascart P. J., Sitnikov M. N., and Voessing H. J.: A numerical study of tropical cross-tropopause transport by convective overshoots during the TROCCINOX golden day, Atmos. Chem. Phys. Discuss., 6, 13 001–13 025, 2006. 6739

Cho, J. Y. N., Newell, R. E., Bui, T. P., et al.: Observations of convective and dynamical instabilities in tropopause folds and theircontribution to stratosphere-troposphere exchange, J. Geophys. Res., 104(D17), 21 549–21 568, 1999. 6745

Corti, T., Luo, B. P., Fu, Q., Vomel, H., and Peter, T.: The impact of cirrus clouds on tropical

troposphere-to-stratosphere transport, Atmos. Chem. Phys., 6, 2539–2547, 2006, http://www.atmos-chem-phys.net/6/2539/2006/. 6739
Davies H. C.: A lateral boundary formulation for multilevel prediction models, Q. J. R. Meteorol. Soc., 102, 405–418, 1976. 6748
Dessler, A. E. and Yang, P.: The Distribution of Tropical Thin Cirrus Clouds Inferred from Terra MODIS Data, J. of Climate, 16, 1241–1247, 2003. 6742
Di donfrancesco G., Cairo, F., Buontempo, C., et al.: Balloonborne Lidar for cloud physics studies, Appl. Opt., 42, 22, 5701–5708, 2006. 6744
Durry, G., Huret, N., Hauchecorne, A., et al.: Isentropic advection and convective lifting of water vapor in the UT – LS as observed over Brazil (22° S) in February 2004 by in situ high-resolution measurements of H2O, CH4, O3 and temperature, Atmos. Chem. Phys. Discuss., 6, 12 469–12 501, 2006. 6745, 6752
Folkins I. and Martin R. V.: The vertical structure of tropical convection and its impact on the budgets of water vapor and ozone, J. Atmos. Sci., 62, 1560–1573, 2005. 6738
Fueglistaler, S., Bonazzola, M., Haynes, P. H., Peter, T.: Stratospheric water vapor predicted from the Lagrangian temperature history of air entering the stratosphere in the tropics, J. Geophys. Res., 110, D08107, doi:10.1029/2004JD005516, 2005. 6746
Fueglistaler, S. and Fu, Q.: Impact of clouds on radiative heating rates in the tropical lower stratosphere, J. Geophys. Res., 111, D23202, doi:10.1029/2006JD007273, 2006. 6739
Gettelman, A., Salby, M. L., and Sassi, F.: Distribution and influence of convection in the tropical tropopause region, J. Geophys. Res.-Atmos., doi:1029/2006JD004080, 1737–1746, 2002. 6739
Hartmann, R. L.: Radiative effects of clouds on Earth's climate. Aerosol-Cloud-Climate Interactions,International Geophysical Series, 54, Academic Press, edited by: Hobbs, P. V., 151–173, 1993. 6738
Kain, J. S. and Fritsch, J. M.: A one-dimensional entraining/detraining plume model and its application in convective parameterization, J. Atmos. Sci., 47, 2784–2802, 1990. 6748
Kain, J. S. and Fritsch, J. M.: Multiscale Convective Overturning in Mesoscale Convective Systems: Reconciling Observations, Simulations, and Theory, Mon. Wea. Rev., 126, 2254–2273, 1998.
Kain, J. S.: The Kain-Fritsch convective parametrization: an update. J. App. Meteorol., 43, 170–181, 2004. 6748
King, M. A., Chee, S., Platinick, S. E., Wang, M., and Liou, K.: Cloud Retrieval Algorithms for

MODIS: Optical Thickness, Effective Particle Radius, and Thermodynamic Phase, Algorithm Theoretical Basis Document No. ATBD-MOD-MOD06 Cloud product, 1997.
Lehman, R.: On the choice of relaxation coefficients for Davies' lateral boundaries scheme for regional weather prediction models, Meteorol. Atmos. Phys., 52, 1–14, 1993. 6748
Liou, K.-N.: Influence of cirrus clouds on weather and climate processes: A global perspective, 1986, Mon. Wea. Rev., 114, 1167–1200, 1986. 6738
Liu, L. and Mishchenko, M. I.: Constraints on PSC particle microphysics derived from lidarobservations, J. Quantitative Spectroscopy Radiative Transfer, 70, 817–831, 2001. 6745
Liu, C. and Zipser, E. J.: Global distribution of convection penetrating the tropical tropopause, J. Geophys. Res., 110, D23104, doi:10.1029/2005JD006063, 2005. 6741
Luo, B. P., Peter, T., Wernli, H., et al.: Ultrathin Tropical Tropopause Clouds: II. Stabilization mechanisms, Atmos. Chem. Phys., 3, 1093–1100, 2003, http://www.atmos-chem-phys.net/3/1093/2003/. 6740
Mace, G. G., Zhang, Y., Platnick, S., King, M. D., Minnis, P., and Yang, P.: Evaluation of Cirrus Cloud Properties Derived from MODIS Data Using Cloud Properties Derived from Ground-Based Observations Collected at the ARM SGP Site, J. Appl. Meteorol., 44, 221–240, 2005. 6742
Mace, G. G., Benson, S., and Vernon, E.: Cirrus Clouds and the Large-Scale Atmospheric State: Relationships Revealed by Six Years of Ground-Based Data, J. Climate, 19, doi:10.1175/JCLI3786.1, 3257–3278, 2006. 6753
Mackenzie, A. R., Schiller, C., Peter, T., et al.: tropopause and hygropause variability over the equatorial Indian Ocean during February and March 1999, J. Geophys. Res. 111, D18112, doi:10.1029/2005JD006639, 2006. 6740
Marecal, V., Durry, G., Longo, K., Freitas, S., Riviere, E. D., and Pirre, M.: Mesoscale modelling of water vapour in the tropical UTLS: two case studies from the HIBISCUS campaign, Atmos. Chem. Phys. Discuss., 6, 8241–8284, 2006, http://www.atmos-chem-phys-discuss.net/6/8241/2006/. 6743, 6751, 6752
Marti, L. and Mauersberger, K.: A survey and new measurements of ice vapor pressure at temperatures between 170 and 250 K, Geophys. Res. Lett., 20, 363–366, 1993. 6747
Massie, S., Gettelman, A., Randel, W., and Baumgardner, D.: Distribution of tropical cirrus in relation to convection, J. Geophys. Res., 107(D21), 4591, doi:10.1029/2001JD001293, 2002 6740
McFarquhar, G. M. and Heymsfield, A. J.: Microphysical characteristics of three anvils sampled

during the Central Equatorial Pacific Experiment, J. Atmos. Sci., 53, 2401–2423, 1996 6740
Morcrette, J. J., Clough, S. A., Mlawer, E. J., and Iacono, M. J.: Impact of a validated radiative transfer scheme, RRTM, on the ECMWF model climate and 10-day forecasts. ECMWF Technical Memo., 252, 1998. 6749
Mullendore, G. L., Durran, D. R., and Holton, J. R.: Cross.tropopause tracer transport in midlatitude convection, J. Geophys. Res., 116, D06113, doi:10.129/2004JD005059, 2005. 6749, 6750
Noel, V., Winker, D. M., McGill, M., and Lawson, P.:Classification of particle shapes from lidar depolarization ratio in convective ice clouds compared to in situ observations during CRYSTAL-FACE, J. Geophys. Res., 109, D24213, doi:10.1029/2004JD004883, 2004. 6746
Peter, T., Luo, B. P., Flueglistaler, S., et al.: Dehydration potential of ultrathin clouds at the tropical tropopause, Geophys. Res. Lett., 33, 11-1–11-4, 2003. 6740
Pfister, L., Selkirk, H. B., Jensen, E. J., et al.: Aircraft observations of thin cirrus clouds near the tropical tropopause, J. Geophys. Res., 106(D9), 9765–9786, 2001. 6740, 6745, 6746, 6753, 6754
Pommereau J.-P., Garnier, A., Held, G., et al.: An overview of the HIBISCUS campaign, Atmos. Chem. Phys. Discuss., 7, 2389–2475, 2007, http://www.atmos-chem-phys-discuss.net/7/2389/2007/. 6739, 6741
Pressman, D. J.: Chislennaja model' gidrotermicheskikh processov v pochve kak chast' skhemy mezomasshtabnogo prognoza (A numerical model of hydrothermical processes in soil as a part of a mesoscale weather forecast scheme). Meteorologiya i gidrologiya, Meteorology and Hydrology, 11, 62–75, 1994 (in Russian). 6749
Ritter, B. and Geleyn, J.: A comprehensive radiation scheme for numerical weather prediction models with potential applications in climate simulations, Mon. Wea. Rev., 120, 303–325, 1992. 6749
Sassen, K. and Benson, S.: A Midlatitude Cirrus Cloud Climatology from the Facility for Atmospheric Remote Sensing. Part II: Microphysical Properties Derived from Lidar Depolarization, J. Atmos. Sci., 58, 2103–2112, 2001. 6745
Santacesaria, V., Carla, V., Mackenzie, R., et al.: Clouds at the tropical tropopause: A case study during the APE-THESEO campaign over the western Indian Ocean, J. Geophys. Res., 108(D2), 4044, doi:10.1029/2002JD002166, 2003. 6740
Saunders, R. and Brunel, P.: RTTOV 8.5 user guide, EUMETSAT SAFNWP http://www.metofce.gv.uk/research/interproj/nwpsaf/rtm/, 2004. 6750

Schultz, P.: An explicit cloud physics parameterization for operational numerical weather prediction, Mon. Wea. Rev., 123, 3331–3343, 1995.
Stohl, A., Haimberger L., Scheele M. P., and Wernli, H.: An intercomparison of results from three trajectory models, Meteorol. Appl., 127–135, 1999. 6746
Tompkins, A. M., Gierens, K., and Radel, G.: Ice Supersaturation in the ECMWF Integrated Forecast System, ECMWF technical memorandum, 481, 2005. 6748
Whiteway, J., Cook, C., Gallagher, M., et al.: Anatomy of cirrus clouds: Results from the Emerald airborne campaigns, Geophys. Res. Lett., 31, L24102, doi:10.1029/2004GL021201, 2004. 6746
Zampieri, M., Buzzi A., and Malguzzi, P.: Sensitivity of quantitative precipitation forecasts to boundary layer parameterization: a flash flood case study in the Western Mediterranean, Nat. Hazards Earth Syst. Sci., 5, 603–612, 2005, http://www.nat-hazards-earth-syst-sci.net/5/603/2005/. 6749

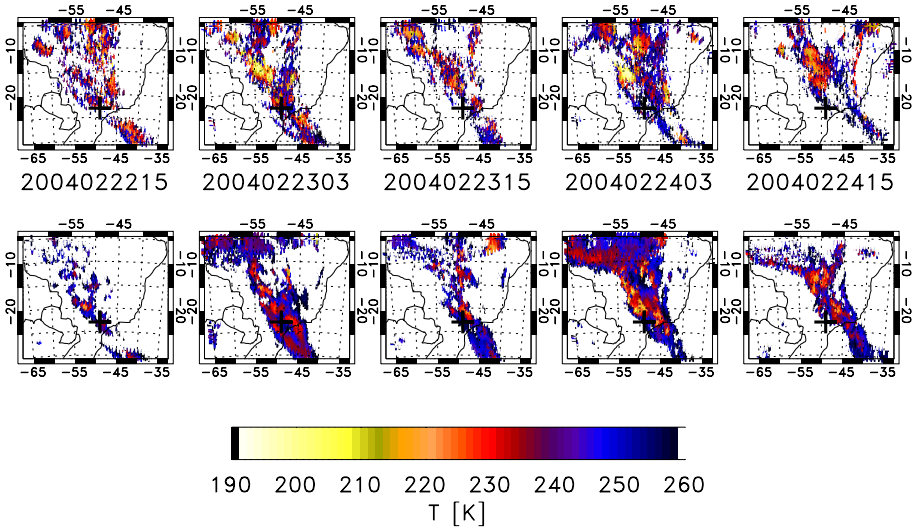

Fig. 1. Above: from left to right, infrared radiance temperature from GOES-12 10.7 μm channel from 22 February 15:00 UTC, to 23 February 15:00 UTC. The position of SF4 flight is indicated with the black cross. Below: as above, but for infrared radiance temperature retrieved from BOLAM mesoscale model with RTTOV forward model.

ACPD
7, 6737–6765, 2007

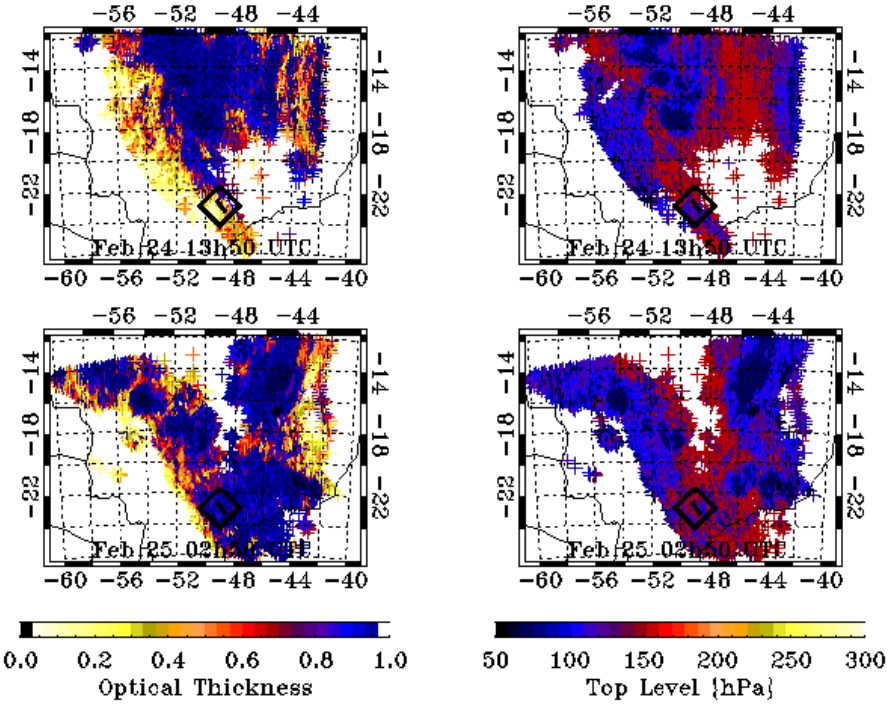

Fig. 2. Left: optical thickness estimated by MODIS imager onboard the TERRA satellite on 24 January 13:00 UT (above) and on 25 January 01:00 UT (below). The balloon position lies within the black box. Right: as left but for cloud top height.

ACPD
7, 6737–6765, 2007

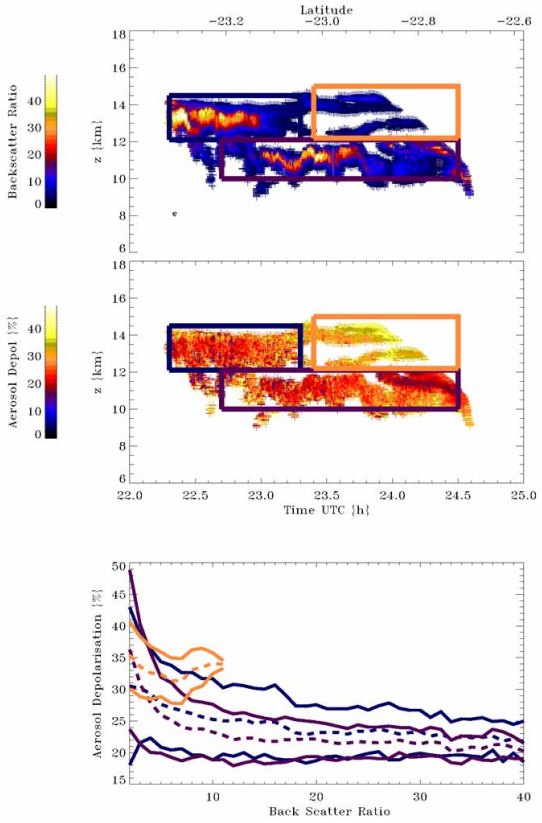

Fig. 3. Above: aerosol backscatter ratio at 532 nm (BSR) function of the flight time and height. The cirrus layers are enclosed in colored boxes as described in the text. Middle: same as above but for aerosol depolarization.Below: Aerosol backscatter ratio versus depolarization. Colors identify cirrus layers 1–3 (see text); dashed lines are the average D values, and solid lines the standard deviation.

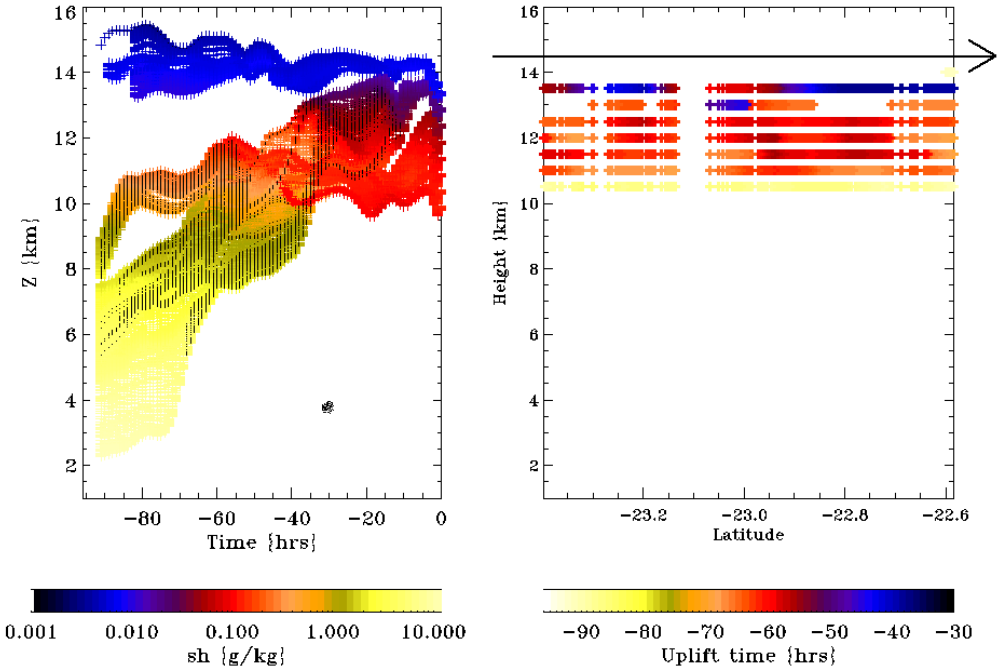

Fig. 4. Left: Cirrus airmass back-trajectory time evolution as a function of height. Colors are the specific humidity interpolated along the trajectory from ECMWF fields. Small dots indicate where the ice saturation condition is satisfied (RH_i >100%). Right: convective uplift time t_c inferred from the trajectories. The black arrow indicates the SF4 flight direction.

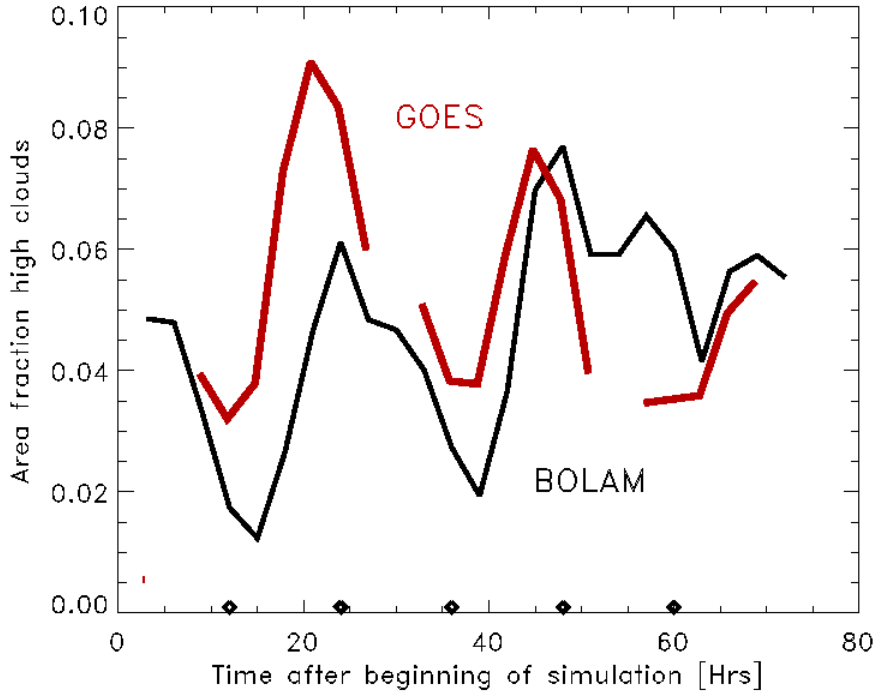

Fig. 5. High cloud area fraction from GOES observations (red line) and BOLAM simulations (black line). The time of the images of Fig. 1 are reported on the x-axis as diamonds.

ACPD
7, 6737–6765, 2007

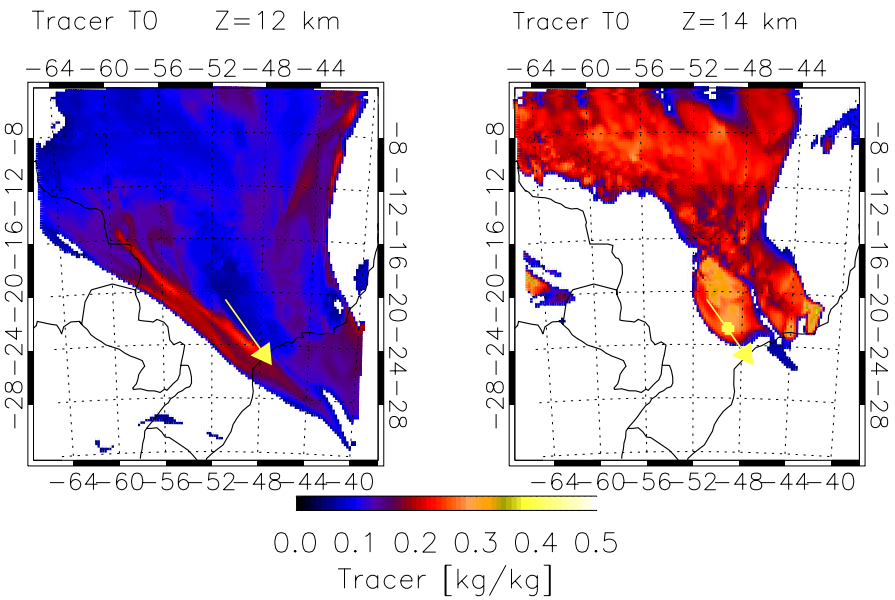

Fig. 6. Left: T0 tracer field at 12 km height simultaneous to flight SF4 (24 February, 23:00 UTC). Flight direction is indicated by the yellow arrow. Right: as left, but for T48 tracer at 14 km height.

ACPD
7, 6737–6765, 2007

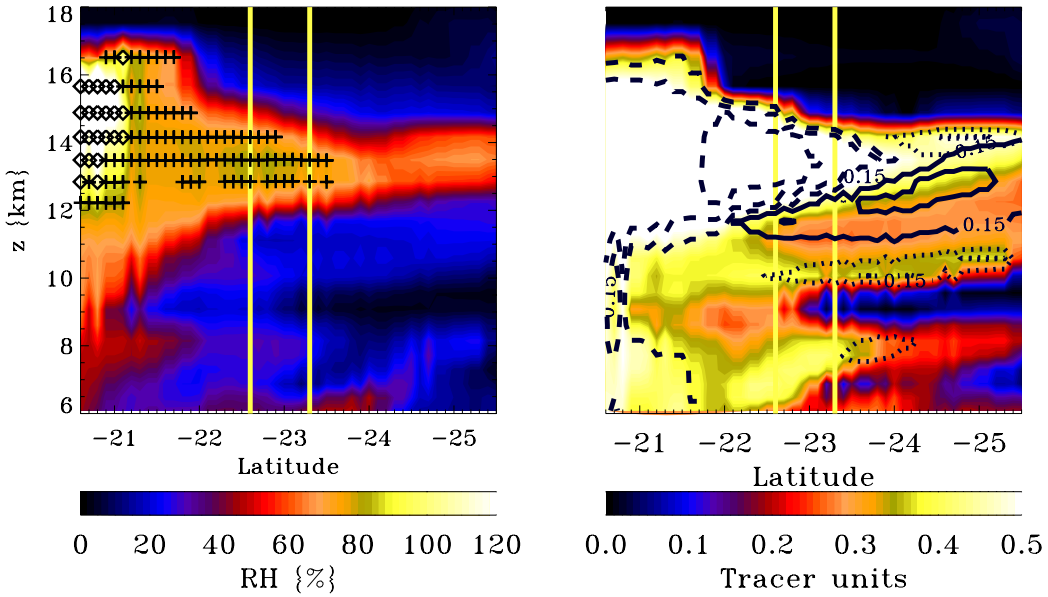

Fig. 7. Left: BOLAM relative humidity on 24 February 23:00 UTC. Latitudinal cross section is oriented along the yellow arrow in Fig. 6. Crosses indicate where supersaturation occurs (RH_i>130%). Right: as left but for BOLAM T0 tracer. Overlaid, contours of T0 (dashed lines), T24 (dotted lines) and T48 (solid lines) for 0.15 and 0.2 kg/kg. In both plots the SF4 latitude range lies between the yellow bars.

ACPD
7, 6737–6765, 2007

EGU